13th International Symposium on Turbulence and Shear Flow Phenomena (TSFP13)
Montreal, Canada, June 25–28, 2024

THE INFLUENCE OF WINDWARD AND EFFECTIVE SLOPE ON TURBULENT CHANNEL FLOW OVER RATCHET ROUGHNESS

Oleksandr Zhdanov
James Watt School of Engineering
University of Glasgow
Glasgow, United Kingdom, G12 8QQ
oleksandr.zhdanov@glasgow.ac.uk

Thomas O. Jelly
Department of Mechanical Engineering
University of Melbourne
Melbourne, Victoria, 3010, Australia
tom.jelly@unimelb.edu.au

Angela Busse
James Watt School of Engineering
University of Glasgow
Glasgow, United Kingdom, G12 8QQ
angela.busse@glasgow.ac.uk

ABSTRACT

Ratchet roughness is the simplest example of 2D directional roughness that breaks forward-backward symmetry due to the imbalance between the slope of its windward and leeward oriented faces. As a result, the fluid dynamic properties of these surfaces depend on the sign of the mean flow direction. In the present study, the influence of the windward slope and effective slope of ratchet-type roughness on the mean flow and turbulence statistics is investigated. To this end, direct numerical simulations of turbulent channel flow at friction Reynolds number 550 are conducted for a series of systematically varied ratchet surfaces. The results show that roughness function and mean flow and turbulence statistics strongly depend on the windward and effective slopes of ratchet-type surfaces. The roughness function increases with increasing windward slope for a fixed effective slope value. The roughness effect also depends on the effective slope, but this dependence is more complex in comparison. Deviation from outer-layer similarity is influenced both by effective and windward slope, with a stronger effect observed for longer ratchets. Windward and effective slope also leave a clear imprint on the streamwise energy spectra and quadrant statistics.

INTRODUCTION

Directional roughness is a special class of surface roughness that encompasses anisotropic surfaces of different kinds, such as riblet surfaces, surfaces composed of transverse and longitudinal bars or elongated roughness elements, and irregular surfaces with significant differences in their streamwise and spanwise correlation lengths (Chung *et al.*, 2021). The fluid dynamic behaviour of such surfaces depends on the flow direction relative to the dominant direction of the surface, e.g., streamwise-aligned bars result in a lower roughness effect compared to their spanwise-aligned counterpart (Orlandi & Leonardi, 2006).

Most directional forms of roughness studied to date preserve forward-backward symmetry, i.e., the flow statistics are invariant to a change in sign of the mean flow direction. An example of directional roughness that breaks forward-backward symmetry are ratchet surfaces which are composed of spanwise aligned bars with scalene triangular cross-section. For these surfaces, depending on the sign of the mean flow direction, the flow will encounter windward surfaces with high or low slopes. Examples of ratchet-type roughness include sand dunes and ripples, fish scales, and some forms of ocean waves.

The study by Jiang *et al.* (2018) demonstrated that the orientation of ratchet-type roughness influences large-scale convective structures and global heat transport. Similar surfaces are also studied in river hydrodynamics and overland flows in the context of flow structures over large-scale river dunes and barchan dunes (e.g., Wiggs & Weaver, 2012; Dey *et al.*, 2020). However, roughness effects of ratchet-type surfaces have received considerably less attention. Busse & Zhdanov (2022*a*,*b*) reported for direct numerical simulations (DNS) of turbulent channel flow strong dependence of the mean flow and turbulence statistics on the orientation of ratchet-type surfaces with respect to the mean flow direction. The roughness function of surfaces with high slope sections facing the mean flow significantly exceeded the values obtained for the same surfaces but with the low-slope faces exposed to the flow.

In previous research on rough-wall turbulence, the streamwise effective slope ES (Napoli *et al.*, 2008)

$$ES = \frac{1}{A}\int_A \left| \frac{\partial H(x,y)}{\partial x} \right| dxdy, \tag{1}$$

where $H(x,y)$ is the roughness height map, A is the planform area of the surface, and x is the streamwise and y the spanwise coordinate, has been identified as a key topographical parameter that influences the roughness effect of a surface (Chung *et al.*, 2021). However, existing predictive correlations based on ES fail to capture the roughness effect of ratchet surfaces, since the effective slope is insensitive to the imbalance between leeward and windward slope that is characteristic of ratchet roughness. Even correlations that take the windward slope explicitly into account, e.g., the Sigal-Danberg parameter (Sigal & Danberg, 1990; Van Rij *et al.*, 2002), demonstrate poor performance.

Table 1. Parameters for the direct numerical simulations: L_x, L_y, and L_z are domain sizes in the streamwise, spanwise, and wall-normal directions; N_x, N_y, and N_z are the number of grid points in the streamwise, spanwise, and wall-normal directions; N_r is the number of ratchets placed on each channel wall; Δx^+ and Δy^+ is the viscous scaled grid spacing in the streamwise and spanwise directions; Δz^+_{min} and Δz^+_{max} are the minimum and maximum viscous scaled grid spacing in the wall-normal direction.

Case	$L_x \times L_y \times L_z$	$N_x \times N_y \times N_z$	N_r	N_x/N_r	Δx^+	Δy^+	Δz^+_{min}	Δz^+_{max}
$s/h = 4$	$6.4\delta \times 3.2\delta \times 2.08\delta$	$2560 \times 384 \times 576$	20	128	1.375	4.58	0.67	< 5.0
$s/h = 8$	$6.4\delta \times 3.2\delta \times 2.08\delta$	$1280 \times 384 \times 576$	10	128	2.75	4.58	0.67	< 5.0
$s/h = 12$	$6.72\delta \times 3.36\delta \times 2.08\delta$	$896 \times 384 \times 576$	7	128	4.125	4.81	0.67	< 5.0

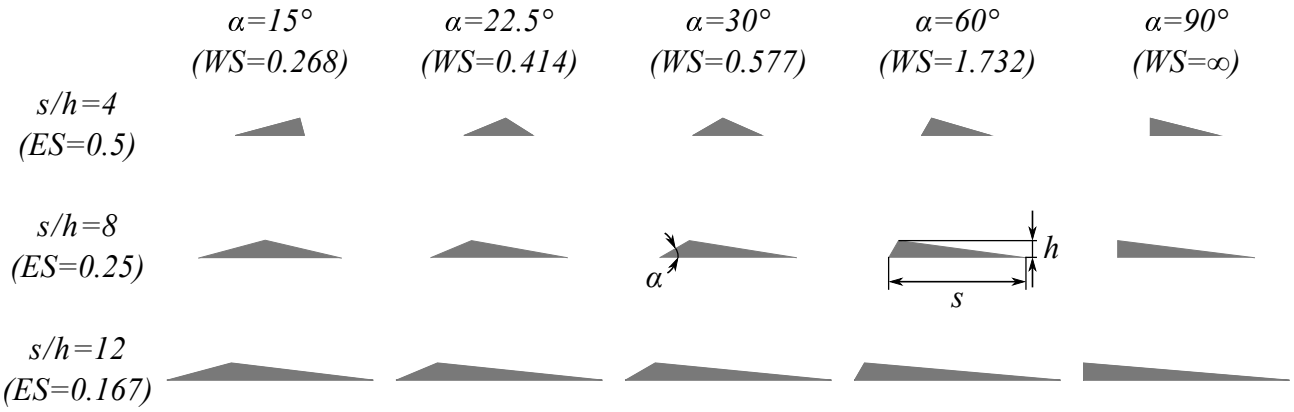

Figure 1. Schematic illustration of the studied ratchet configurations and their basic geometric parameters. Only one ratchet per case is shown. $WS = \tan(\alpha)$ is the windward slope and ES is the effective slope.

The windward slope (WS) for ratchets composed of triangular bars is equal to the tangent of an angle α formed by its windward side and base, while the effective slope, for fully covered ratchet surfaces, is related to the ratchet length s and ratchet height h as $ES = 2h/s$. The focus of the current study is to systematically explore the dependency of the roughness effect on the windward slope of the ratchet, which influences the upward deflection of the mean flow, and on the effective slope, which determines the distance between ratchet crests. To this end, a series of DNS are conducted to obtain mean flow properties and turbulence statistics, including Reynolds and dispersive stresses and quadrant maps of turbulent velocity fluctuations. A further aim is to lay the basis for improved predictive correlations for rough surfaces that can take into account a break in forward-backward symmetry.

METHODOLOGY

Ratchet surfaces are generated by fully covering both walls of a channel with spanwise bars of scalene triangular cross-section. In total, fifteen different ratchet-type surfaces are considered in this study (Figure 1). The ratchet height (h) is set to 0.08δ in all cases, where δ is the mean channel half-height. The ratchet spacing (s) is systematically varied from $4h$ to $12h$, which correspond to the ES range from 0.5 to 0.167. For each spacing five values of windward slope angle α are considered (15°, 22.5°, 30°, 60°, and 90°).

For each surface, a DNS of incompressible fully developed turbulent channel flow is performed using the code iIMB (Busse *et al.*, 2015). The flow is driven through the channel by a constant (negative) mean streamwise pressure gradient, which determines the mean friction velocity (u_τ). All simulations are performed at friction Reynolds number ($Re_\tau = u_\tau\delta/\nu$, where ν is the kinematic viscosity) of 550. Depending on the ratchet length, the streamwise (L_x) and spanwise (L_y) domain size is set to either $6.4\delta \times 3.2\delta$ or $6.72\delta \times 3.36\delta$ to fit a natural number of ratchets. The ratchets are placed on both channel walls and the ratchet pattern on the upper wall is shifted by $s/2$ to minimise any local blockage effects. The reference plane $z = 0$ corresponds to the mean roughness height resulting in a mean channel height of 2δ for all cases.

The ratchet geometry is resolved using an iterative version of the embedded boundary method by Yang & Balaras (2006) and ratchet surfaces are treated as no-slip walls. Periodic boundary conditions are imposed in the streamwise and spanwise directions. Uniform grid resolution is applied in the streamwise and spanwise directions ($\Delta x^+, \Delta y^+ < 5.0$). The streamwise grid spacing is adjusted depending on the value of s to maintain a constant resolution of each ratchet with 128 grid points, i.e., $s/\Delta x = 128$ in all cases. In the wall-normal direction, uniform grid spacing ($\Delta z^+_{\text{min}} = 0.67$) is applied up to the ratchet crest, while above it gradually increases up to the maximum value ($\Delta z^+_{\text{max}} < 5.0$) at the channel centreplane. In all simulations, the flow statistics are acquired for a minimum of 57 flow through times after the initial transient. The statistical quantities are computed using the double-averaging approach of Raupach & Shaw (1982).

RESULTS

Mean velocity profiles

The double-averaged mean streamwise velocity profiles for all cases are plotted in Figure 2a together with the smooth-wall data at the same Reynolds number. In all roughness cases, a zero-plane displacement (z_{off}) is applied to recover the expected log-law slope of the profiles. The values of z_{off} are

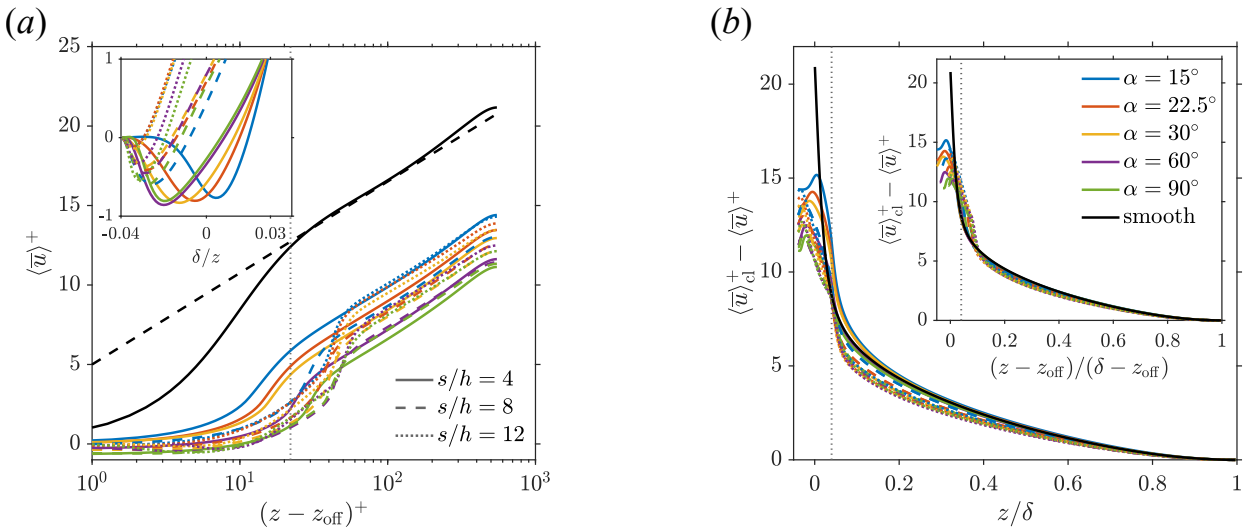

Figure 2. (a) Mean streamwise velocity profiles. The black dashed line shows the smooth wall log-law $\langle\overline{u}\rangle^+ = \kappa^{-1}\ln z^+ + A$, with von Kármán constant $\kappa = 0.4$ and log-law intercept $A = 5.0$. (b) Velocity-defect profiles. The inset shows velocity-defect profiles with applied zero-plane offset. The thin dotted vertical line indicates the height of the ratchet crests in all panels.

included in Table 2. A substantial downward shift in the log-law region is observed for all ratchet-type surfaces. For fixed effective slope, increasing windward slope induces an increase in the downward shift in all cases, indicating that higher α at $ES = const$ results in a larger mean momentum deficit. Below the ratchet crest, a reverse flow is observed within the cavity formed between the windward and leeward sides of adjacent ratchets (see inset in Figure 2a). The size and shape of the reverse flow region is strongly dependent on both the effective and windward slopes of the surface. In addition, for medium ($s/h = 8$) and long ($s/h = 12$) ratchets the strength of reverse flow is affected by the windward slope, while for short ratchets ($s/h = 4$), the strength of reverse flow is relatively insensitive to this parameter.

When plotted against z/δ, the outer-layer similarity of the mean velocity profile is affected in most cases (see Figure 2b), with stronger deviation observed for larger s/h values, i.e., lower ES. Application of z_{off} significantly improves the collapse of velocity defect profiles (see inset in Figure 2b). Compared to the short and medium ratchets ($s/h \leq 8$, $ES \leq 0.25$), where the collapse extends almost down to the ratchet crest, long ratchets ($s/h = 12$, $ES \leq 0.167$) exhibit inferior collapse for all windward slopes. Moreover, for surfaces composed of long ratchets the recovery of outer-layer similarity depends on the windward slope, with superior outer-layer similarity observed for low α, where better collapse with the smooth-wall data is observed down to lower wall-normal locations. These results are consistent with previous study on ratchet-type roughness at $Re_\tau = 395$ by Busse & Zhdanov (2022*a*).

Roughness function

The roughness function ΔU^+ was determined as the downward shift of the rough-wall log law relative to the smooth-wall log law and is presented in Figure 3 and Table 2. All tested surfaces demonstrate strong dependence of their roughness effect on both windward and effective slope with the strongest effect of α observed for the shortest ratchets. ΔU^+ progressively increases with α for all tested s/h values, but the rate of increase is not constant across tested range with higher rate observed from $\alpha = 15°$ to $\alpha = 30°$. In this region the increase is close to linear in all s/h cases, while for $\alpha \geq 60$

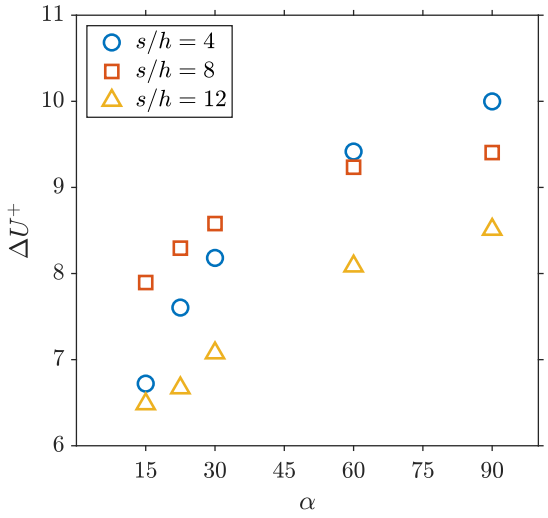

Figure 3. Roughness function plotted versus windward slope angle.

the roughness effect starts to saturate, i.e., the rate of increase drops. The dependency of ΔU^+ on the effective slope is more complex. For high α, the roughness function increases, as expected, with increasing effective slope. However, for low to moderate α ($15° \leq \alpha \leq 30°$) the highest ΔU^+ values are observed for the medium effective slope case ($s/h = 8$).

These results reinforce that empirical correlations based on orientation insensitive parameters, such as effective slope, rms roughness height, skewness, etc, cannot give accurate predictions for ratchet-type roughness. In addition, there is also no simple linear dependency of ΔU^+ on WS. For example, using the correlation developed by De Marchis (2016):

$$\Delta U^+ = \frac{1}{\kappa}\ln(ES \cdot Sq^+) + B, \qquad (2)$$

where Sq is the rms roughness height (here: $Sq = h/(2\sqrt{3})$) and $B = 3.5$ is an empirical constant, the predicted values of

Table 2. Values of the roughness function ΔU^+, zero-plane displacement z_{off}, equivalent sand-grain roughness k_s/k, and Sigal-Danberg parameter Λ_s.

α	ΔU^+	z_{off}/δ	k_s/k	Λ_s
$s/h = 4, ES = 0.5$				
15°	6.72	0.020	1.36	34.77
22.5°	7.60	0.015	1.93	18.60
30°	8.18	0.013	2.43	12.13
60°	9.42	0	3.98	5.04
90°	10.00	-0.012	5.03	4.00
$s/h = 8, ES = 0.25$				
15°	7.90	-0.010	2.17	69.55
22.5°	8.29	-0.025	2.54	37.20
30°	8.58	-0.032	2.85	24.25
60°	9.23	-0.037	3.70	10.07
90°	9.40	-0.032	3.96	8.00
$s/h = 12, ES = 0.167$				
15°	6.48	-0.034	1.23	104.32
22.5°	6.67	-0.036	1.33	55.80
30°	7.07	-0.042	1.56	36.38
60°	8.09	-0.046	2.34	15.11
90°	8.51	-0.040	2.77	12.00

ΔU^+ are 8.12, 6.39, and 5.37 for surfaces with $ES = 0.5$, $ES = 0.25$, and $ES = 0.167$, irrespective of α. For the long and medium ratchets, the predicted values underestimate the roughness effect in all cases, and for the short ratchet cases, a good match is only obtained for the case $\alpha = 30°$, i.e., the configuration where windward and leeward slope have similar magnitude. We would expect for the empirical correlation to give good results for ratchets with a nearly isosceles cross-section. While this is the case for $s/h = 4$, $\alpha = 30°$, the roughness function is significantly underpredicted for the $s/h = 8$, $\alpha = 15°$ case, which is also close to an isosceles shape.

The correlation developed by Sigal & Danberg (1990) takes into consideration windward and leeward oriented surface faces in the definition of the eponymous parameter Λ_s, which for the present surfaces is computed as:

$$\Lambda_s = \frac{A_t}{A_f}\left(\frac{A_f}{A_w}\right)^{-1.6}, \tag{3}$$

where A_t is the plan area of roughness elements, A_f is their frontal projected area, and A_w is their windward wetted surface area. The values of Λ_s for the present cases are included in Table 2. Since the Sigal-Danberg relationship predicts the equivalent sand-grain roughness k_s, this parameter was estimated from the present values of ΔU^+ obtained at a single

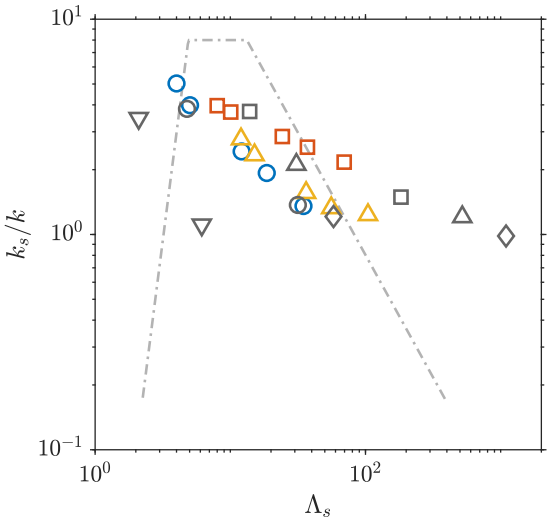

Figure 4. Estimate of the equivalent sand-grain roughness k_s as a function of the Sigal-Danberg parameter Λ_s. Present data is shown with coloured symbols and $s/h(E/S)$ values are as in Figure 3. Grey symbols show data from Busse & Zhdanov (2022*a*). The same symbol styles correspond to the same $s/h(E/S)$ values, data for $s/h = 2(ES = 1)$ is shown with ▽ and data for $s/h = 16(ES = 0.125)$ with ◇. The grey dash-dotted line shows the Sigal & Danberg (1990) relationship for 2D roughness.

Re_τ using the relationship discussed by Chung *et al.* (2021):

$$\frac{k_s}{k} = \frac{\exp(\kappa(\Delta U^+ - A + B_s(\infty)))}{k^+}, \tag{4}$$

where, $k = h$ and $A - B_s(\infty) \approx 3.5$. The estimated equivalent sand-grain roughness values (see Table 2) are compared to the Sigal-Danberg relationship for 2D roughness in Figure 4. In addition, the data from Busse & Zhdanov (2022*a*) for ratchet-type roughness has been included. For all tested s/h values, k_s/k appears to decrease almost linearly with Λ_s (in log scales), however the slope is non-linearly dependent on the effective slope, complicating the development of predictive correlations. The Sigal-Danberg relationship does not give accurate predictions for most of the surfaces, with a few exceptions, namely for short ratchets with high α and medium and long ratchets with $\alpha = 22.5°$. The inability of the Sigal-Danberg relationship to capture the roughness effect of ratchet-type surfaces can be explained by the background of this relationship. Sigal & Danberg intended low Λ_s values to represent dense roughness composed of square bars, while high Λ_s were to cover sparse roughness cases, whereas for the present study 100% planform solidity is maintained in all cases. In addition, none of the data used by Sigal & Danberg was for an orientation-dependent two-dimensional roughness case.

The data by Busse & Zhdanov (2022*a*) obtained at $Re_\tau = 395$ shows a good agreement with the present results for surfaces with the same effective slope. In addition, for some cases it provides insight in the behaviour of k_s/k over a larger range of Λ_s, which is directly dependent on α at constant s/h. In particular, for long ratchets it can be observed that k_s/k saturates at high Λ_s, i.e., as α is decreased. In none of the present cases, k_s/k drops significantly below 1, whereas based on Sigal & Danberg (1990) a continued decrease would be expected

as Λ_s is increased.

Although it is not expected that correlations based solely on surface windward face angles can give accurate predictions for ratchet-type surfaces, since their roughness effect also depends on the effective slope, we tested the correlation developed by Bons (2005), which predicts k_s/k based on the average forward facing surface angle $\overline{\alpha}_f$ as: $k_s/k = 0.0191\overline{\alpha}_f^2 + 0.0736\overline{\alpha}_f$ (here: $\alpha = \overline{\alpha}_f$). This correlation significantly overpredicts k_s for all cases (not shown). However, the correlation by Bons (2005) was developed using data on turbine blade roughness with low $\overline{\alpha}_f$ ($\overline{\alpha}_f < 12^\circ$) and therefore is not intended to cover high $\overline{\alpha}_f$.

Quadrant statistics and spectra

As is evident from the mean velocity profiles in Figure 2a there is a region of mean reverse flow in the cavity between ridges. This is illustrated for a representative case ($s/h = 8$ and $\alpha = 30^\circ$) in Figure 5a, which shows the time- and phase-averaged wall-normal velocity field with superimposed mean-flow streamlines. The size of the recirculation zone depends on the windward slope and effective slope, where the latter determines the leeward slope of the ratchet at fixed ES. For cases with short ratchets recirculation zone occupies almost the entire cavity, while for long ratchets it is significantly reduced and confined to the bottom of the cavity for all α (not shown).

From Figure 5a a gradual downwards motion of the mean flow can be observed above the leeward slope of the surface, which is compensated by a more pronounced upward flow deflection over the windward ratchet face. This corresponds to the location of the highest levels of time-averaged Reynolds shear stress (see Figure 5b). While for almost the entire domain $\overline{u'w'} < 0$, high positive values for $\overline{u'w'} \gg 0$ occur over the windward facing slope towards the ratchet crest. The prevalence of different types of events that make a contribution to $\overline{u'w'}$, is presented in Figures 5c–f, which show the local probability of Q1 (outward interactions), Q2 (ejections), Q3 (inward interactions), and Q4 (sweeps), respectively. Sweeps and ejections dominate over the leeward slope of the ratchet, with a dominance of ejections over sweeps in the area of the flow associated with the recirculation zone. The high positive values over the windward slope of the ratchets arise from outward and inward interaction with the latter being dominant toward the ratchet crest. The observations made are part of an ongoing analysis of the data, and the dependency of the aforementioned observation on ES and WS have yet to be fully determined.

Premultiplied streamwise energy spectra ($k_x\phi_{uu}/u_\tau^2$) for all surfaces with $s/h = 8$ are presented in Figure 6 together with reference smooth-wall data. In all roughness cases the energy peak is located below the ratchet crest. The ratchet pattern wavelength leaves a clear imprint in the spectra, since the maximum energy levels are localized at the same wavelength. As ratchet windward face angle is increased from 15° to 60° the magnitude of this peak also increases, followed by a slight drop at $\alpha = 90^\circ$, which is accompanied by the emergence of a second peak located at higher wavelength and closer to the crest. However, in all ratchet cases, the peak magnitude is significantly reduced compared to the smooth-wall case. Spectra for further Reynolds stresses and the two other s/h series of cases are part of an ongoing investigation.

CONCLUSIONS

The present DNS results demonstrate the influence of both windward and effective slope on the roughness effect of ratchet surfaces. At constant effective slope, in the range of low windward slope angles, ΔU^+ increases linearly with α, whereas for high windward slope ΔU^+ starts to saturate. In most cases, existing predictive correlations, including those that take into account windward surface area or slope angle, do not give satisfactory predictions for this type of surface. Increase in ratchet length leads to reduced levels of outer-layer similarity, which can be improved by application of a zero-plane displacement; however, for the longest tested ratchets outer-layer similarity cannot be fully recovered. The mean flow field shows a separation region in all cases, but the extent of this region depends both on ES and WS. Preliminary results for the medium ratchets show that ejection and sweep events dominate over most of the flow domain and take their highest values over the leeward side of the ratchet. Outward and inward interactions make only a small contribution in most areas, however, they prevail over the windward face of the ratchet. Similarly, a clear imprint of the ratchet length can be observed in the premultiplied spectra which also change as the windward face angle is increased. In the next stage of this ongoing study, global and local flow statistics will be considered, including further analysis of Reynolds stress spectra and quadrant statistics. The adaptation of existing predictive correlations by introducing a slope-imbalance parameter will also be attempted.

ACKNOWLEDGEMENTS

We gratefully acknowledge support by the United Kingdom's Engineering and Physical Sciences Research Council (grant number EP/V002066/1) and access to the ARCHER2 UK National Supercomputing Service via the UK Turbulence Consortium (grant number EP/X035484/1).

REFERENCES

Bons, J. 2005 A critical assessment of reynolds analogy for turbine flows. *Journal of Heat and Mass Transfer* **127** (5), 472–485.

Busse, A., Lützner, M. & Sandham, N. D. 2015 Direct numerical simulation of turbulent flow over a rough surface based on a surface scan. *Computers & Fluids* **116**, 129–147.

Busse, A. & Zhdanov, O. 2022*a* Direct numerical simulations of turbulent channel flow over ratchet roughness. *Flow, Turbulence and Combustion* **109** (4), 1195–1213.

Busse, A. & Zhdanov, O. 2022*b* The structure of turbulent channel flow over ratchet-type roughness. In *Proceedings of the 12th International Symposium on Turbulence and Shear Flow Phenomena (TSFP-12)*.

Chung, D., Hutchins, N., Schultz, M. P. & Flack, K. A. 2021 Predicting the drag of rough surfaces. *Annual Review of Fluid Mechanics* **53**, 439–471.

De Marchis, M. 2016 Large eddy simulations of roughened channel flows: Estimation of the energy losses using the slope of the roughness. *Computers & Fluids* **140**, 148–157.

Dey, S., Paul, P., Ali, Sk. Z. & Padhi, E. 2020 Reynolds stress anisotropy in flow over two-dimensional rigid dunes. *Proceedings of the Royal Society A* **476** (2242), 20200638.

Jiang, H., Zhu, X., Mathai, V., Verzicco, R., Lohse, D. & Sun, C. 2018 Controlling heat transport and flow structures in thermal turbulence using ratchet surfaces. *Physical Review Letters* **120** (4), 044501.

Napoli, E., Armenio, V. & De Marchis, M. 2008 The effect of the slope of irregularly distributed roughness elements on turbulent wall-bounded flows. *Journal of Fluid Mechanics* **613**, 385–394.

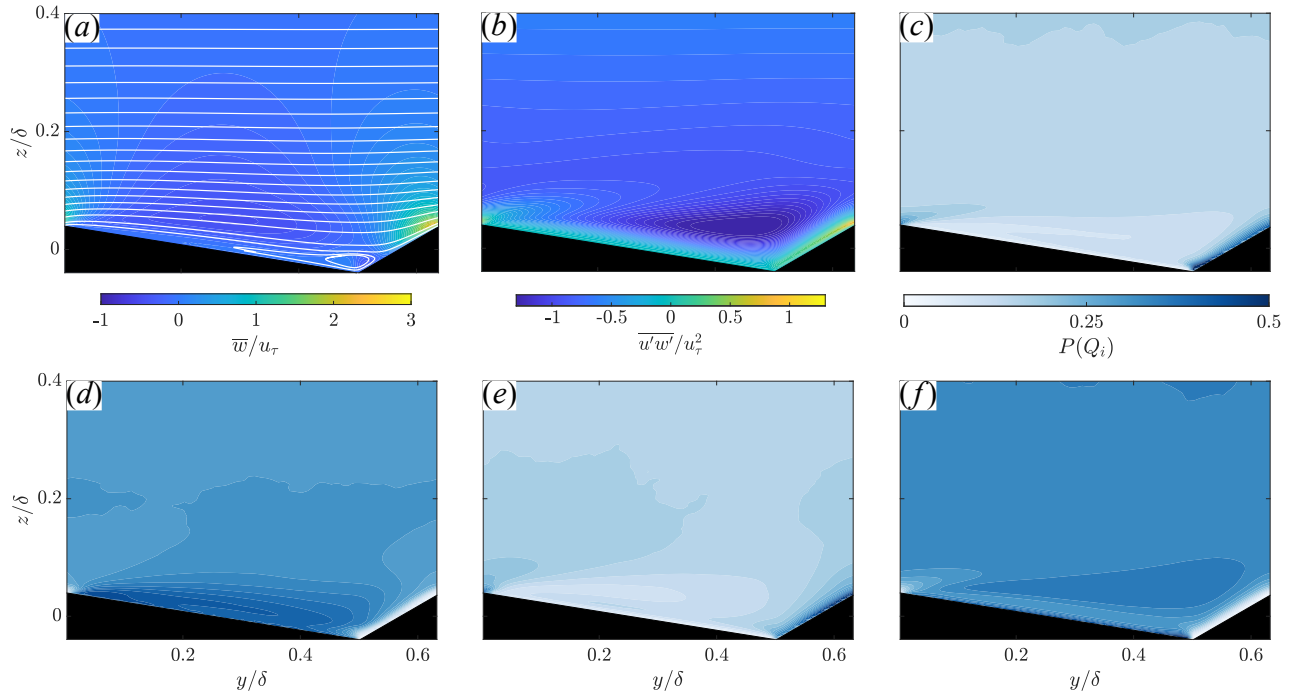

Figure 5. Ratchet roughness with $s/h = 8$ and $\alpha = 30°$: (a) time- and phase-averaged wall-normal velocity field with superimposed mean-flow streamlines; (b) time- and phase-averaged Reynolds shear stress field; probability of different quadrant events: (c) Q1 (outward interactions), (d) Q2 (ejections), (e) Q3 (inward interactions), (f) Q4 (sweeps). The mean flow direction is from left to right.

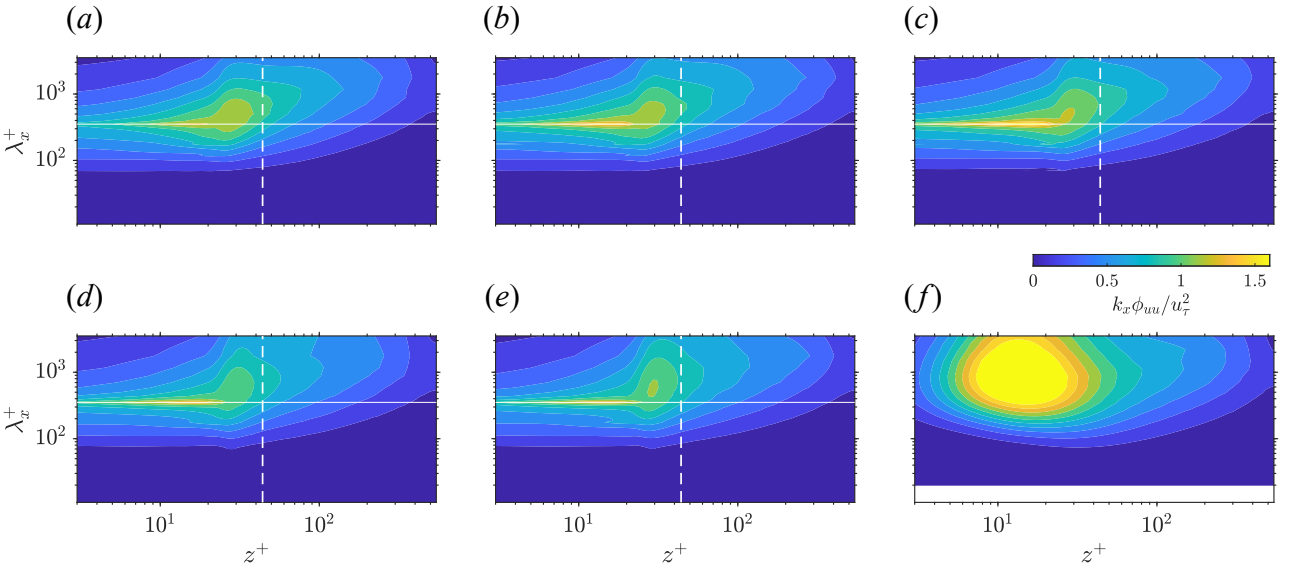

Figure 6. Premultiplied streamwise energy spectra $k_x\phi_{uu}/u_\tau^2$ as a function of streamwise wavelength (λ_x) and wall-normal location (z) for surfaces with fixed $s/h = 8$ and windward slope (a) $\alpha = 15°$, (b) $\alpha = 22.5°$, (c) $\alpha = 30°$, (d) $\alpha = 60°$, and (e) $\alpha = 90°$. The thin white vertical dashed line marks the wall-normal location of the ridge crest and the thin white horizontal line marks the ratchet wavelength. Reference smooth-wall data is shown in (f).

Orlandi, P. & Leonardi, S. 2006 DNS of turbulent channel flows with two-and three-dimensional roughness. *Journal of Turbulence* (7), N73.

Raupach, M.R. & Shaw, R.H. 1982 Averaging procedures for flow within vegetation canopies. *Boundary-Layer Meteorology* **22** (1), 79–90.

Sigal, A. & Danberg, J.E. 1990 New correlation of roughness density effect on the turbulent boundary layer. *AIAA Journal* **28** (3), 554–556.

Van Rij, J.A., Belnap, B.J. & Ligrani, P.M. 2002 Analysis and experiments on three-dimensional, irregular surface roughness. *Journal of Fluids Engineering* **124** (3), 671–677.

Wiggs, G.F.S. & Weaver, C.M. 2012 Turbulent flow structures and aeolian sediment transport over a barchan sand dune. *Geophysical Research Letters* **39** (5).

Yang, J. & Balaras, E. 2006 An embedded-boundary formulation for large-eddy simulation of turbulent flows interacting with moving boundaries. *Journal of Computational Physics* **215** (1), 12–40.